Eur. Phys. J. A (2025) 61:57
https://doi.org/10.1140/epja/s10050-025-01521-9

THE EUROPEAN
PHYSICAL JOURNAL A

Regular Article - Experimental Physics

Proton capture on ^{90}Zr revisited

A. Simon[1,a], **J. Koros**[1], **O. Olivas-Gomez**[1], **R. Kelmar**[1], **E. Churchman**[1,4], **A. M. Clark**[1], **C. Harris**[2,3], **S. L. Henderson**[1], **S. E. Kelly**[1], **P. Millican**[1], **A. Palmisano-Kyle**[2,3], **C. S. Reingold**[1], **D. Robertson**[1], **E. Stech**[1], **A. Spyrou**[2,3], **W. P. Tan**[1]

[1] Department of Physics and Astronomy, University of Notre Dame, Notre Dame, IN 46556, USA
[2] National Superconducting Cyclotron Laboratory, Michigan State University, East Lansing, MI 48824, USA
[3] Department of Physics and Astronomy, Michigan State University, East Lansing, MI 48824, USA
[4] *Present Address:* University of North Carolina at Chapel Hill, Chapel Hill, NC 27599, USA

Received: 30 August 2024 / Accepted: 20 February 2025

Communicated by Aurora Tumino

Abstract The ^{90}Zr(p,γ)^{91}Nb reaction is one of the important reactions in the $A \approx 90$ mass region and part of the nucleosynthesis path responsible for production of ^{92}Mo during the γ-process. Discrepant data in the literature provide a cross section that varies up to 30% within the Gamow window for the ^{90}Zr(p,γ)^{91}Nb reaction. Thus, the cross section measurements of ^{90}Zr(p,γ)^{91}Nb reaction were revisited using the γ-summing technique. The results are consistent with the lower-value cross sections found in the literature. Based on the new data an updated reaction rate for ^{90}Zr(p,γ)^{91}Nb is provided that is up to 20% higher than that obtained from the NON- SMOKER code.

1 Introduction

The origin of the 35 p-nuclei, the proton-rich isotopes of heavy elements that cannot be produced by the s- or r-processes remains an open question in nuclear astrophysics. The γ-process proposed by Woosley [1] consists of a series of photodisintegration reactions on seed s-process nuclei and reproduces well the solar abundances of the p-nuclei. The main challenge of the model is the underproduction of the Mo isotopes, which could stem from either the uncertainties of the astrophysical models or nuclear physics inputs. One of the reactions that impact the nucleosynthesis process in the Mo region is ^{90}Zr(p,γ)^{91}Nb, which has been investigated by several authors.

The first measurement by Roughton et al. [2] measured the astrophysical reaction rate directly via the activation technique by irradiating a thick zirconium target. The results obtained from the thick-target method cannot be directly compared with cross section measurements, as they provide an integrated cross section measurement. Additionally, the activation method can only be applied to the capture to the metastable state as the ground state of ^{91}Nb has a half-life or 680 years. However, theoretical calculations of the reaction rate from the work of Spyrou et al. [3], resulted in a rate that was in agreement with that from [2].

Those two data sets do not agree with two other measurements of the ^{90}Zr(p,γ)^{91}Nb reaction that were obtained using in-beam γ spectroscopy. The results of Laird et al. [4] and Erbacher et al. [5] give a cross section about 30% lower than that from Spyrou et al. at energies just above the Gamow window for the ^{90}Zr(p,γ)^{91}Nb reaction.

In this work, the ^{90}Zr(p,γ)^{91}Nb was revisited to resolve the discrepancy between the existing data. The γ-summing technique, as in the case of the measurement of Spyrou et al. was used here. In Sect. 2, details of the experimental procedure are outlined, in Sect. 3 the cross sections obtained in this work are presented and a comparison of the current work with the previous measurements is provided in Sect. 4. In Sect. 5, a comparison to Hauser-Feshbach model calculations is given and a reaction rate based on the current results is presented.

2 Experimental procedure

The experiment was performed at the Nuclear Science Laboratory [6] at the University of Notre Dame. A proton beam produced by the 10-MV FN tandem at energies between 2.8–6 MeV was impinged on an enriched (98(1)%) target of ^{90}Zr, with a thickness of 969(48) μg/cm^2. The same target was used in the measurement of Spyrou et al. [3]. The energy spread of the beam from the accelerator is about 5 keV, the energy loss in the target ranged from 34 to 66 keV for the highest and lowest beam energy utilized, respectively.

---

[a] e-mail: anna.simon@nd.edu (corresponding author)

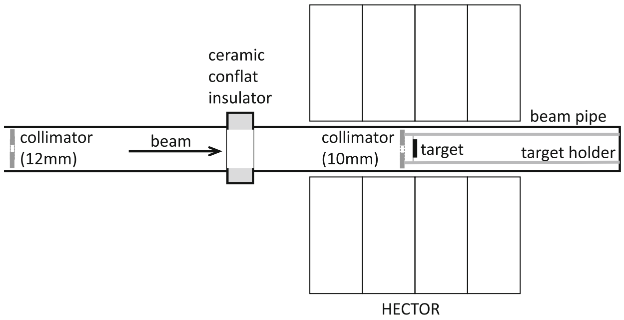

Fig. 1 Sketch of the experimental setup used in this work

The target was placed at the center of HECTOR [7,8], the High Efficiency TOtal absorption spectrometeR. HECTOR is a NaI(Tl) array comprised of 16 segments providing a nearly 4π solid angle coverage for γ-ray detection.

The beam pipe surrounding the target was electrically insulated from the beam pipe upstream and from the detector, and was utilized as a Faraday cup for measurements of the beam current. The current was constantly monitored through the experiment and the total charge deposited into the Faraday cup was recorded using a charge integrator.

Two collimators were used for tuning the beam, a 12 mm collimator about 2 m upstream from the target and a 10 mm collimator about 10 mm in front of the target. The 10 mm collimator was insulated from the beam pipe during beam tuning and was reconnected as a part of the Faraday cup during data taking. This was to prevent δ-electrons from suppressing the beam current reading. A sketch of the experimental setup is shown in Fig. 1.

3 Results

The γ rays from the deexcitation cascade following the proton capture were detected in HECTOR. The excited state populated via the proton capture is well defined and given by:

$$E_X = E_{CM} + Q, \tag{1}$$

where E_{CM} is the total kinetic energy in the center of mass frame and $Q = 5.154$ MeV is the reaction Q-value. Thus, the total energy carried by the γ rays in the deexcitation cascade is $E_\Sigma = E_X$. The events where the whole cascade is absorbed by the detector form the sum peak, a peak corresponding to the E_Σ energy. In such case, the capture cross section for the reaction of interest can be obtained from:

$$\sigma = \frac{N_\Sigma}{N_t N_b \varepsilon}, \tag{2}$$

where N_Σ is the number of counts within the sum peak, N_t is the target areal density, N_b is the number of beam particles impinged on the target and ε is the summing efficiency.

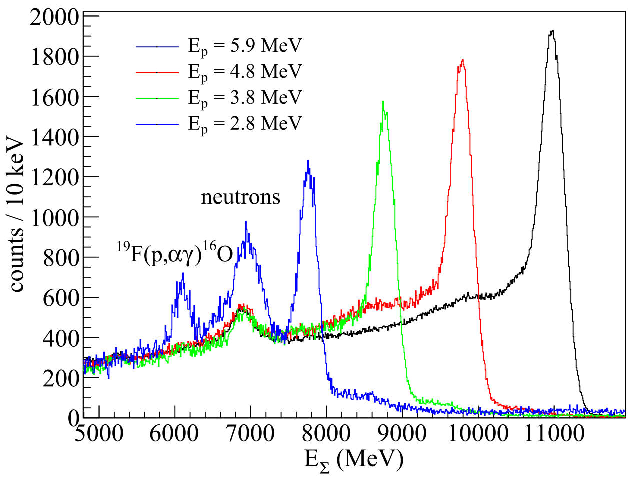

Fig. 2 Sample sum spectra for ^{90}Zr(pγ)^{91}Nb reaction obtained with HECTOR

Sample sum spectra obtained in this work for 2.8, 3.8, 4.8 and 5.9 MeV proton energies are shown in Fig. 2. For clarity of presentation the spectra have been scaled to the same background level at γ-ray energy of 5 MeV. In each spectrum a sum peak is clearly visible at the far-right end of the histogram.

The peak at 6.9 MeV is due to neutrons interacting with the NaI(Tl) crystal and resulting in a sum peak following the ^{127}I(n,γ)^{128}I reactions within the crystal. The Q-value for neutron capture on ^{127}I is 6.9 MeV and the capture cross section is the highest for thermal neutrons. Thus, once the neutrons thermalize in the detector crystals and are captured into iodine the result is a sum peak at E_Σ of 6.9 MeV. The high-energy tail of the sum-peak can be attributed to the proton-capture reaction on other isotopes of Zr in the target. In particular, the Q-value for the ^{92}Zr(p,γ)^{93}Nb is 6.04 MeV, i.e., 890 keV higher than that for the ^{90}Zr(p,γ)^{91}Nb reaction, thus the visible structure could be attributed to this reaction.

The spectrum for a proton energy of 2.8 MeV shows two additional lines, at 6.1 and 6.9 MeV resulting from the ^{19}F(p,$\alpha\gamma$)^{16}O reactions. The ^{19}F is a common contaminant present in target materials. The cross section for the ^{19}F(p,$\alpha\gamma$)^{16}O reaction is well known [9] and increases by a factor of two once the beam energy falls below 2.8 MeV. Thus, the 6.1 and 6.9 MeV lines are present in the spectrum obtained with $E_p = 2.8$ MeV, where the effect is additionally enhanced due to a much higher beam current used during data collection and the rapidly decreasing cross section for the reaction of interest. At higher beam energies, the lines from the ^{19}F(p,$\alpha\gamma$)^{16}O reaction are dominated by the incomplete summation events from the primary reaction. The contaminants present in the target limited the range of the proton energies covered in this work to 2.8 MeV and above, so that

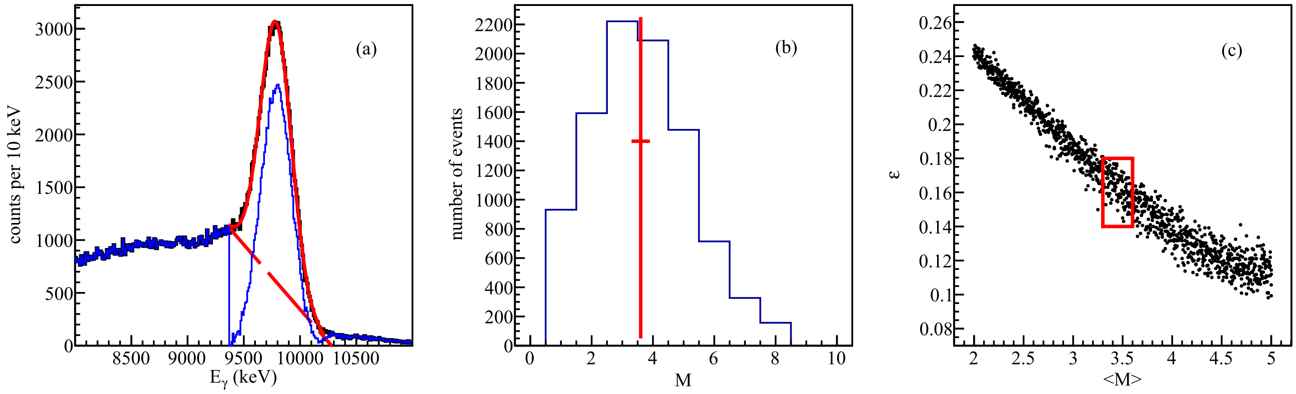

Fig. 3 Example of the analysis procedure shown for a 9.9 MeV sum peak from the ^{90}Zr(pγ)^{91}Nb reaction: **a** fit to the experimental sum peak (solid red line), subtracted background (dashed red line) and resulting sum peak (blue). **b** Experimental segment multiplicity distribution with a mean value $\langle M \rangle$ and its uncertainty marked with red lines. **c** Efficiency curve for a 9.9 MeV sum peak obtained from Geant4 simulations. The red rectangle indicates the uncertainty in the determined efficiency

the sum peak did not overlap with the lines from the contaminants.

The analysis procedure followed the steps described in detail in Olivas-Gomez et al. [8] and is briefly summarized here. For each beam energy, the sum peak is fitted with a combination of a Gaussian peak and a linear background to account for incomplete summation events. Then the linear background is subtracted from the sum-peak and the resulting spectrum is integrated within $\pm\, 3\sigma$ range around the centroid of the sum-peak. An example fit for a sum peak at 9.9 MeV is shown in Fig. 3a.

The summing efficiency was determined using Geant4 simulations. γ-ray cascades corresponding to a total energy equal to E_Σ were used to model the detector response. A combination of cascades with varying number of γ rays was used in each simulation. This provided an input to the simulation that reproduces the large variety of cascades that are likely to originate from the compound nucleus populated in the experiment without making any assumptions on the properties of the nucleus. For each E_Σ, 1000 simulations were performed with combinations of cascades resulting in average γ-ray multiplicities ranging from 1–6 to provide an efficiency curve within the multiplicity range relevant to the experiment. The Geant4 simulations followed the procedures described in [10].

To relate the properties of the simulated cascades to experimental observables, the average segment multiplicity $\langle M \rangle$ of the events within the sum peak was determined. Segment multiplicity M is the number of HECTOR segments that detected a γ-ray signal. The average segment multiplicity was calculated as a mean of the M distribution with the uncertainty calculated as the standard deviation of the mean. The same quantity can be derived for experimental data, providing means to relate simulations to the experimental results. The simulated summing efficiency for each sum peak energy measured experimentally can thus be plotted as a function of $\langle M \rangle$. The summing efficiency for a given E_Σ can then be determined from that plot for the value of $\langle M \rangle$ obtained from the experiment, and its uncertainty is estimated from the range of ε values corresponding to the uncertainty range in the experimental value of $\langle M \rangle$. A sample of the analysis process for a sum peak at 9.9 MeV is shown in Fig. 3.

Table 1 Cross section data for the ^{90}Zr(p,γ)^{91}Nb obtained in this work. The uncertainty of the E_{lab} and E_{CM} is 5 keV

E_{lab} (MeV)	E_{CM} (MeV)	E_{eff} (MeV)	σ (mb)
6.00	5.93	5.90 ± 0.034	9.31 ± 1.14
5.80	5.74	5.70 ± 0.036	8.04 ± 0.99
5.40	5.34	5.30 ± 0.036	5.95 ± 0.73
5.20	5.14	5.10 ± 0.042	5.1 ± 0.63
5.00	4.95	4.90 ± 0.044	4.24 ± 0.52
4.80	4.75	4.71 ± 0.040	3.57 ± 0.44
4.50	4.45	4.40 ± 0.046	2.62 ± 0.32
4.30	4.25	4.20 ± 0.051	2.09 ± 0.26
4.00	3.96	3.91 ± 0.051	1.34 ± 0.16
3.80	3.76	3.71 ± 0.052	1.12 ± 0.14
3.60	3.56	3.51 ± 0.047	0.707 ± 0.087
3.40	3.36	3.31 ± 0.051	0.523 ± 0.064
3.20	3.16	3.11 ± 0.055	0.376 ± 0.046
3.20	3.16	3.11 ± 0.055	0.368 ± 0.045
3.00	2.97	2.91 ± 0.057	0.264 ± 0.033
2.80	2.77	2.70 ± 0.066	0.158 ± 0.019

The primary source of uncertainty in the cross-section calculations stems from the efficiency simulations. The relative uncertainty of the simulated efficiency is 10–12%. The beam current was measured with a Faraday cup with an uncertainty of 5% and the target thickness is known with a 5% uncertainty.

The cross section data for ^{90}Zr(p,γ)^{91}Nb reaction obtained in this work are listed in Table 1 and are presented in Fig. 4.

4 Comparison with previous measurements

A comparison of the results of the current work with cross section data for ^{90}Zr(p,γ)^{91}Nb found in the literature is presented in Fig. 4. An excellent agreement between the current results and those from [4,5] can be seen. The results of Spyrou et al. deviate from other measurements at energies above 3.3 MeV. The activation results of Roughton et al. are in agreement with current measurements if both the ^{90}Zr(p,γ)^{91}Nb and ^{91}Zr(p,n)^{91}Nb reactions are taken into account, as discussed in [5]. Results from Roughton et al. [2] are not shown here, as no cross section was reported by the authors, but instead the reaction rate was calculated from the measured thick-target yields.

Figure 5 shows a ratio of the results from Spyrou et al. to those from the current work. To compute the ratio, a fit was performed to the current data and was then interpolated to the E_{CM} values of the Spyrou results. It can be seen that the three lowest-energy points from [3] are in an excellent agreement with the current work. At about 3.3 MeV, the ratio between the two data sets begins to increase and reaches a factor of 1.5 for the last five data points. It is speculated that the discrepancy stems from issues with the beam current readings for the data from [3]. At the highest beam energies, where the beam current on target was limited to about 1 nA due to the rates in the summing detector, a small unsupressed collimator was used immediately upstream of the detector and the beam was defocused further upstream to help reduce the beam current on target. It is likely that the δ electrons resulting from the beam hitting the collimator made it to the Faraday cup and suppressed the true reading of the beam current. As such the reduced current reading would artificially increase the calculated cross section. The effect decreases with the decreasing beam energy, as the beam current on target was increased to compensate for the decreasing reaction cross section. This was achieved by improving the beam focus which may have reduced the amount of beam hitting the collimator and thus reduced the flux of δ electrons. The first beam tune adjustment in the Spyrou data was done prior to the measurement of the 4 MeV point (indicated in Fig. 5) and reduced the flux of δ electrons. A beam retune prior to the measurement of the lowest energy points that were measured last most likely resolved the issue. During the measurements with HECTOR, beam was retuned every two energy steps.

It is important to note that the deviation between the data sets cannot be attributed to the calculations of the summing efficiency of the SuN detector used in [3]. A deviation of 30% in the efficiency could only be achieved if the average segment multiplicity was miscalculated in the analysis by at least one segment. Since for the SuN detector this value is obtained as a Gaussian fit to the segment multiplicity distribution, this would result in a clear shift of the Gaussian peak relative to the distribution of the experimental data. As such, the findings of this paper have no impact on other results from SuN or recent reanalysis of the ^{90}Zr(p,γ)^{91}Nb data by Palmisano-Kyle et al. [12]. The findings of this paper do not affect other capture measurements obtained with the SuN detector. For example the measurements of ^{90}Zr(α,γ)^{91}Nb cross section obtained with SuN [13] and with HECTOR [14] are in an excellent agreement with each other, as shown in [14].

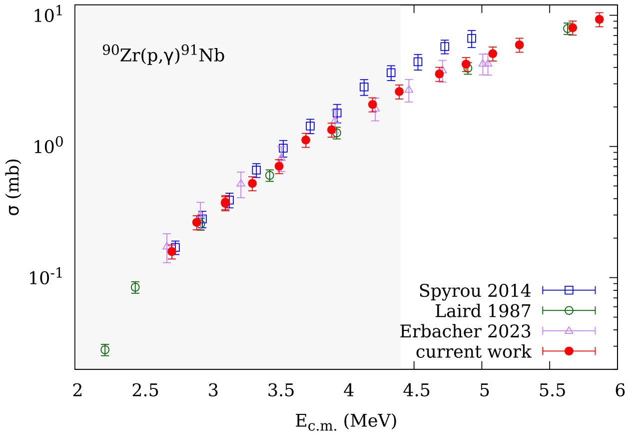

Fig. 4 Reaction cross section for ^{90}Zr(pγ)^{91}Nb obtained in this work (solid red circles) compared to the previous measurements found in the literature. The light-gray rectangle indicates the Gamow window for the γ-process

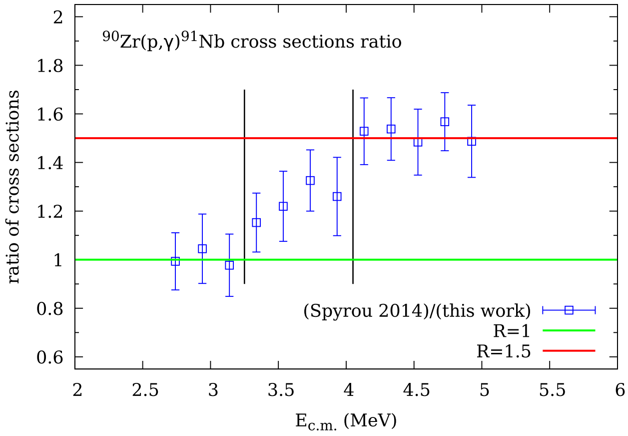

Fig. 5 Ratio of the cross section for ^{90}Zr(pγ)^{91}Nb measured by Spyrou et al. [3] to the current results obtained with HECTOR. Dashed vertical lines indicate beam retune in Spyrou data

5 Discussion

The experimental results of this work were used to determine the best theoretical description of reaction cross section for ^{90}Zr(p,γ)^{91}Nb using the Hauser-Feshbach (HF) formalism. TALYS 1.9 code [15] was used to explore combination of various models for level density (LD) and γ-ray strength function (gSF) to calculate the reaction cross section. The range of pre-

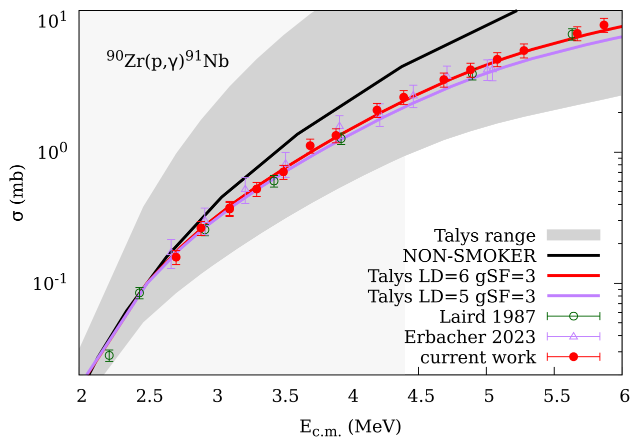

Fig. 6 Hauser-Feshbach models of the reaction cross section for ^{90}Zr(pγ)^{91}Nb compared to the experimental data. TALYS LD = 6 gSF = 3 (solid red line) represents the best fit to the data obtained in this work, TALYS LD = 5 gSF = 3 (dashed purple line) corresponds to the best fit obtained in [5]. Black solid line shows the cross sections from NON-SMOKER [11]. The dark gray area indicates the range of predictions from TALYS when all possible combinations of LD and gSF models are utilized. The light-gray rectangle indicates the Gamow window for the γ-process

diction obtained from TALYS for all possible combinations of model inputs for the LD and gSF is shown as a shaded gray area in Fig. 6. A chi-square analysis was performed to identify a model combination that best reproduces the data. The best model combination obtained in this work corresponds to LD model 6 in TALYS, i.e., microscopic LD calculated using the Gogny force [16], and the gSF model 3, i.e., semi-microscopic Hartree-Fock BCS model [17]. For comparison the best fit to the data from Erbacher et al. was LD = 5 and gSF = 3. Cross sections calculated from both model combinations are shown in Fig. 6.

The best model from TALYS was then used to calculate the reaction rate for ^{90}Zr(p,γ)^{91}Nb. The resulting rate is provided in Table 2 and plotted in Fig. 7a for the temperature range of 1.5–3.5 GK that is relevant to the γ-process. The reaction rate corresponding to the NON- SMOKER cross section from [11] was extracted from the REACLIB database [18] and is also shown in Fig. 7a denoted as NS(rath). It can be noticed that the NON- SMOKER rate is lower than that from the current work, even though the reaction cross section obtained from NON- SMOKER is higher than that measured in this work. For cross check, the rate was recalculated from the original NON-SMOKER cross section and the result is shown in Fig. 7a as NS(calc). As anticipated, the recalculated rate is higher than that from the current work.

A ratio of the reaction rate from this work to that of NON-SMOKER was also computed to explore the change in the recommended rate. The results are shown in Fig. 7b. The ratio of the recommended rate from this work to both the NON- SMOKER, NS(rath), and the recalculated rate, NS(calc) is shown. The ratio of NS(calc) to NS(rath) is also shown in Fig. 7b to show the discrepancy between the NON- SMOKER rate given in REACLIB and that recalculated here from the NON- SMOKER cross section. The current rate is about 20% higher than NS(rath) at the upper limit of the temperature range relevant for the γ-process. When compared to the recalculated NON- SMOKER rate NS(calc), the trend is the opposite, at lower temperatures the current rate exceeds that of NON-SMOKER by about 40%, while at the highest temperatures it is about 20% lower than the NS(calc) rate. The shaded areas correspond to the uncertainty in the measured cross section for the ^{90}Zr(p,γ)^{91}Nb reaction that was propagated through the reaction rate calculations.

Table 2 Reaction rate for ^{90}Zr(p,γ)^{91}Nb obtained in this work

T_9 (GK)	$N_A\langle\sigma v\rangle$ (cm^{3}mol^{-1}s^{-1})
0.1	3.054×10^{-28}
0.15	1.806×10^{-22}
0.2	7.874×10^{-19}
0.25	3.044×10^{-16}
0.3	2.859×10^{-14}
0.4	2.178×10^{-11}
0.5	2.435×10^{-09}
0.6	8.745×10^{-08}
0.7	1.506×10^{-06}
0.8	1.558×10^{-05}
0.9	1.105×10^{-04}
1.0	5.855×10^{-04}
1.5	1.649×10^{-01}
2.0	$4.511 \times 10^{+00}$
2.5	$4.192 \times 10^{+01}$
3.0	$2.137 \times 10^{+02}$
3.5	$7.528 \times 10^{+02}$
4.0	$2.083 \times 10^{+03}$
5.0	$1.003 \times 10^{+04}$
6.0	$3.058 \times 10^{+04}$
7.0	$6.229 \times 10^{+04}$
8.0	$9.029 \times 10^{+04}$
9.0	$1.027 \times 10^{+05}$
10.0	$1.002 \times 10^{+05}$

6 Conclusions

In this work the cross section for the ^{90}Zr(p,γ)^{91}Nb reaction was revisited to resolve the discrepancy between the previous measurements of this reaction. The current results are in an excellent agreement with the work of Laird [4] and Erbacher [5]. The discrepancy between the current work and the previous results of Spyrou et al. [3] are most likely due to issues with beam current integration in [3]. Based on the cross sec-

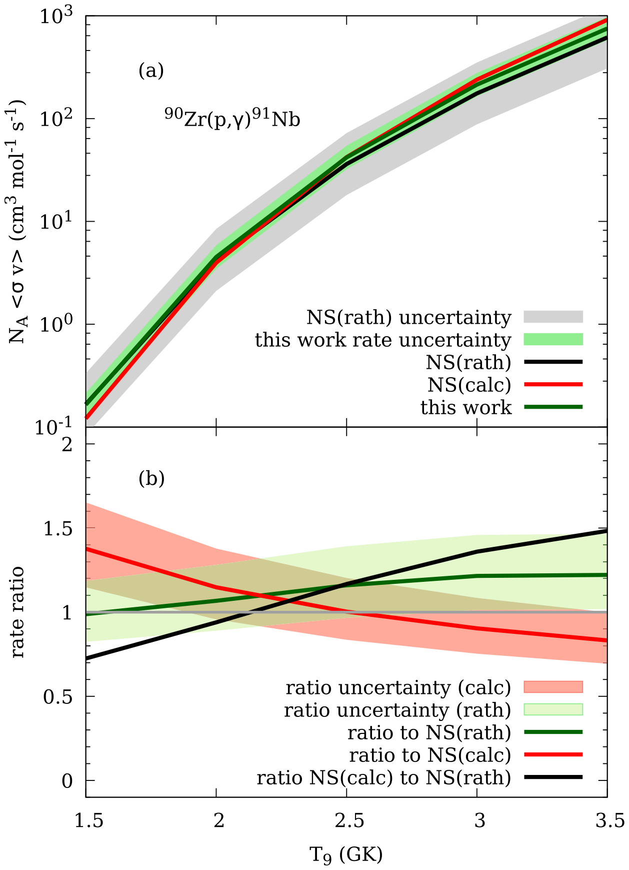

Fig. 7 **a** Reaction rate from this work (solid green line) compared to the NON- SMOKER rate from REACLIB (dashed gray line). The green shaded area represents rate uncertainty from this work, the gray shaded are shows the factor of 2 uncertainty in the NON- SMOKER rate. A rate calculated from the NON- SMOKER cross section is shown as a dashed red line. **b** Ratio of the reaction rate obtained in this work to that from NON- SMOKER (solid green line) and the recalculated NON- SMOKER rate (solid red line). The shaded areas correspond to the uncertainty in the current rate. The dashed black line shows the ration of NS(calc)/NS(rath). The gray line indicates a ratio equal to 1.0 to guide the eye

tion results of this work a new reaction rate for ^{90}Zr(p,γ)^{91}Nb is provided. The rate was calculated using a Hauser-Feshbach model for the cross section obtained with TALYS. The new rate is about 20% higher than that from NON- SMOKER. In order to investigate the impact of the new rate on the models of the γ process, network calculations need to be performed.

Acknowledgements This work was supported by the National Science Foundation under the grants numbers: PHY-1614442, PHY-1713857 and PHY-2310059.

Data Availability Statement Data will be made available on reasonable request. [Author's comment: The data generated during and/or analysed during the current study is available from the corresponding author on reasonable request.]

Code Availability Statement Code/software will be made available on reasonable request. [Author's comment: The code/software generated during and/or analysed during the current study is available from the corresponding author on reasonable request.]

References

1. S.E. Woosley, W.M. Howard, Astrophys. J. Suppl. Ser. **2**, 285 (1978)
2. N. Roughton, M. Fritts, R. Peterson, C. Zaidins, C. Hansen, Atom. Data Nucl. Data Tables **23**(2), 177 (1979). https://doi.org/10.1016/0092-640X(79)90004-4
3. A. Spyrou, S. Quinn, A. Simon, T. Rauscher, A. Battaglia, A. Best, B. Bucher, M. Couder, P. DeYoung, A. Dombos et al., Phys. Rev. C **88**(4), 045802 (2013)
4. C.E. Laird, D. Flynn, R.L. Hershberger, F. Gabbard, Phys. Rev. C **35**, 1265 (1987). https://doi.org/10.1103/PhysRevC.35.1265
5. P. Erbacher, T. Heftrich, A. Endres, J. Glorius, L. Netterdon, D. Just, K. Göbel, M. Krtička, R. Reifarth, K. Sonnabend et al., Eur. Phys. J. A **59**, 69 (2023)
6. Nuclear Science Laboratory, University of Notre Dame. www.isnap.nd.edu (2024)
7. C. Reingold, O. Olivas-Gomez, A. Simon, J. Arroyo, M. Chamberlain, J. Wurzer, A. Spyrou, F. Naqvi, A. Dombos, A. Palmisano et al., Eur. Phys. J. A **55**, 1 (2019)
8. O. Olivas-Gomez, A. Simon, D. Robertson, A. Dombos, F. Streider, T. Kadlecek, M. Hanhardt, R. Kelmar, M. Couder, J. Goerres, et al., in *APS Division of Nuclear Physics Meeting Abstracts*, vol. 2021, pp. FD–005 (2021)
9. P. Cabanelas, J. Cruz, M. Fonseca, A. Henriques, F. Lourenço, H. Luís, J. Machado, J. Pires Ribeiro, A. Sánchez-Benítez, P. Teubig et al., Nucl. Instrum. Methods Phys. Res. Sect. B Beam Interact. Mater. Atoms. **381**, 110 (2016). https://doi.org/10.1016/j.nimb.2016.06.003
10. O. Olivas-Gomez, Constraining the γ-Process Using HECTOR. Phd thesis, University of Notre Dame (2022). https://curate.nd.edu/articles/thesis/Constraining_the_-Process_Using_HECTOR/24825522
11. T. Rauscher, F.K. Thielemann, Atom. Data Nucl. Data Tables **75**(1), 1 (2000). https://doi.org/10.1006/adnd.2000.0834
12. A. Palmisano-Kyle, A. Spyrou, P. DeYoung, A. Dombos, P. Gastis, O. Olivas-Gomez, C. Harris, S. Liddick, S. Lyons, J. Pereira et al., Phys. Rev. C **105**(6), 065804 (2022)
13. S.J. Quinn, A. Spyrou, A. Simon, A. Battaglia, M. Bowers, B. Bucher, C. Casarella, M. Couder, P.A. DeYoung, A.C. Dombos et al., Phys. Rev. C **92**, 045805 (2015). https://doi.org/10.1103/PhysRevC.92.045805
14. R. Kelmar, A. Simon, O. Olivas-Gomez, P. Millican, C.S. Reingold, E. Churchman, A.M. Clark, S.L. Henderson, S.E. Kelly, D. Robertson et al., Phys. Rev. C **101**, 015801 (2020). https://doi.org/10.1103/PhysRevC.101.015801
15. A. Koning, S. Hilaire, S. Goriely, Eur. Phys. J. A **59**(6), 131 (2023). https://doi.org/10.1140/epja/s10050-023-01034-3
16. S. Hilaire, M. Girod, S. Goriely, A.J. Koning, Phys. Rev. C **86**(6), 064317 (2012). https://doi.org/10.1103/PhysRevC.86.064317

17. R. Capote, M. Herman, P. Obložinsk, P. Young, S. Goriely, T. Belgya, A. Ignatyuk, A. Koning, S. Hilaire, V. Plujko et al., Nucl. Data Sheets **110**, 3107 (2009). https://doi.org/10.1016/j.nds.2009.10.004
18. REACLIB Database. https://reaclib.jinaweb.org (2024)